비 선형 유한요소 컴퓨터 프로그램 SMAP-S2의 평가

EVALUATION OF NONLINEAR FINITE
ELEMENT COMPUTER PROGRAM SMAP-S2

김 광 진
COMTEC RESEARCH 사장

개 요

SMAP-S2는 구조물/지반 상호작용에서 기하학적 및 매질의 비선형문제를 해결하기 위해 개발된 2차원 정적 유한요소 프로그램이다. 이 프로그램은 지반공학분야에서 다단계 굴착 또는 성토에 적용하기 편리하다. 이 논문에서는 이론적 배경과 함께 탄소성 모형의 구성방법을 설명하고 해석결과를 실험성과와 비교하였다. 프로그램의 전처리 및 후처리 기능도 설명하였다.

ABSTRACT

SMAP-S2 is an advanced two-dimensional, static finite element computer program developed for the geometric and material nonlinear structure-medium interaction analysis. The program has specific applications for modeling geomechanical problems associated with multi-staged excavation or embankment. Theoretical formulations and computational algorithms are presented along with the description of elasto-plastic material models. Nonlinear features of the code are verified by comparing with known solutions or experimental test results. Capabilities of per- and post-processing programs are discussed.

EVALUATION OF NONLINEAR FINITE ELEMENT COMPUTER PROGRAM SMAP-S2

1. INTRODUCTION

This paper introduces the nonlinear finite element computer program SMAP-S2 developed by COMTEC Research. The program has specific applications for modeling geomechanical problems involving multi-staged excavation or embankment. Other practical applications of SMAP-S2 includes static mechanical analysis for underground structures such as tunnels, shafts, caverns, chambers, etc.

Based on the principle of virtual work, structural equilibrium equations are derived for continuum element, layered reinforced beam element, and truss element. This theoretical formulation takes account of the general nonlinearities associated with large deformation, material inelasticity, and boundary condition change. Verifications are performed to check the nonlinear features of the code by comparing with known solutions or experimental test results.

Material constitutive relationships are presented in a generalized form. The model includes the empirically based Hoek and Brown failure equation for in situ rock mass as well as the classic Von Mises, Mohr-Coulomb, and Drucker-Prager failure equations. The Hoek and Brown model is based on extensive field and laboratory data. The material parameters for this model are tabulated for several different rock types as a function of rock quality. This empirical-based model is very valuable for analyst to model in situ rock mass when the laboratory test data is not sufficient to define the strength properties of in situ rock mass.

The pre- and post-processing capabilities of SMAP-S2 are also discussed. The pre-processor generates nodal coordinates, indexes, and nodal loads for continuum element. And the post-processor produces graphical outputs for stresses, strains, and deformations.

2. FORMULATIONS OF STRUCTURAL EQUILIBRIUM EQUATIONS FOR CONTINUUM ELEMENT

Structural static equilibrium equations can be derived by the principle of virtual work.

$$\int_V \{\delta\bar{\varepsilon}\}^T \{\sigma\}\, dV - \int_S \{\delta u\}^T \{T\}\, dS + \int_V \{\delta u\}^T \rho \{b\}\, dV \qquad (2.1)$$

Where $(\delta\bar{e})$ is the virtual strain corresponding to the virtual displacement $\{\delta u\}$. In the Updated Lagrangian formulation, Equation 2.1 can be approximated in the following incremental form:

$$\int_{V_{n-1}} \{\delta\Delta e\}^T \{\sigma\}_n - \int_{S_\sigma} \{\delta\Delta u\}^T \{T\}_n \, dS + \int_{V_{n-1}} \{\delta\Delta u\}^T \rho \{b\} \, dV \qquad (2.2)$$

Equation 2.2 assumes that the direction and magnitude of the surface loading is independent of the configuration.
The Green-Lagrangian strain increment vector $\{\Delta e\}$ refers to the configuration at load step n-1 and can be decomposed into linear and nonlinear parts.

$$\{\Delta e\} = \{\Delta e^l\} + \{\Delta e^{nl}\} \qquad (2.3)$$

where

$$\Delta e^l_{ij} = \frac{1}{2} (\Delta u_{i,j} + \Delta u_{j,i}) \qquad (2.4)$$

$$\Delta e^{nl}_{ij} = \frac{1}{2} (\Delta u_{k,i} \ \Delta u_{k,j}) \qquad (2.5)$$

The left hand term in Equation 2.2 can be expanded as follows:

$$\int_{V_{n-1}} \{\delta\Delta e\}^T \{\sigma\}_n \, dV = \int_{V_{n-1}} \{\delta\Delta e^l\}^T \{\Delta\sigma\} \, dV + \int_{V_{n-1}} \{\delta\Delta e^{nl}\}^T \{\sigma\}_{n-1} \, dV + \int_{V_{n-1}} \{\delta\Delta e^l\}^T \{\sigma\}_{n-1} \, dV \qquad (2.6)$$

The stress increment vector $\{\Delta\sigma\}$ in Equation 2.6 is related to the linear portion of the Green - Lagrangian strain increment vector.

$$\{\Delta\sigma\} = [D^{ep}] \{\Delta e^l\} \qquad (2.7)$$

Field variables in the above equations can be discretized by the nodal variables. Within each element,

$$\begin{gathered} \{\Delta u\} = [N]_{n-1} \{\Delta\bar{u}\} \\ \{\Delta e^l\} = [B^l]_{n-1} \{\Delta\bar{u}\} \\ \{\Delta e^{nl}\}^T \{\sigma\}_{n-1} = \{\Delta\bar{u}\}^T \left([B^{nl}]^T_{n-1} [\sigma]_{n-1} [B^{nl}]_{n-1} \right) \{\Delta\bar{u}\} \end{gathered} \qquad (2.8)$$

Now substituting Equations 2.6 through 2.8 into 2.2, we obtain the following linearized global equilibrium equation.

$$([K^l] + [K^{nl}]) \{\Delta\bar{U}\} = \{P\}_n - \{R\}_{n-1} \qquad (2.9)$$

where

$$[K^l] = \sum \int_{V_{n-1}} [B^l]^T_{n-1} [D^{ep}] [B^l]_{n-1} \, dV \qquad (2.10)$$

$$[K^{nl}] = \sum \int_{V_{n-1}} [B^{nl}]^T_{n-1} [\sigma]_{n-1} [B^{nl}]_{n-1} \, dV \qquad (2.11)$$

$$\{P\}_n = \sum \int_{S_\sigma} [N]^T_\sigma \{T\}_n \, dS + \sum \int_{V_{n-1}} [N]_{n-1} \rho_{n-1} \{b\} \, dV \qquad (2.12)$$

$$\{R\}_{n-1} = \sum \int_{V_{n-1}} [B^l]^T_{n-1} \{\sigma\}_{n-1} \, dV \qquad (2.13)$$

Two dimensional continuum elements generally include plane strain, plane stress and axisymmetric conditions. Figure 2.1 shows 8 node isoparametric finite element and the corresponding shape functions incorporated into SMAP-S2.

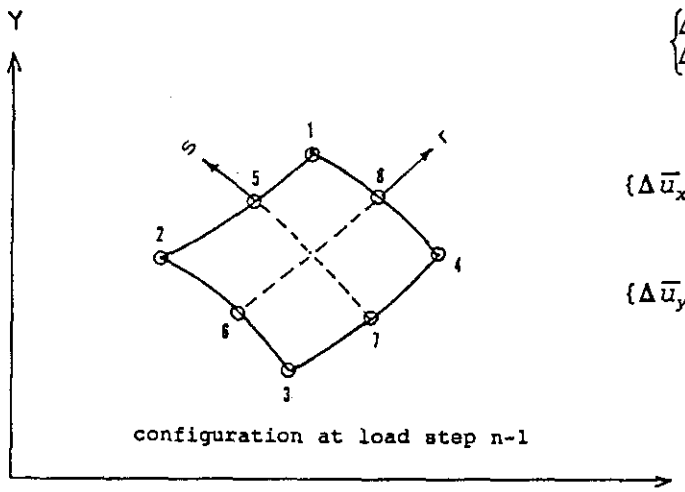

$$\begin{Bmatrix}\Delta u_x\\ \Delta u_y\end{Bmatrix} = \begin{bmatrix}\langle h\rangle & \langle o\rangle\\ \langle o\rangle & \langle h\rangle\end{bmatrix}\begin{Bmatrix}\{\Delta \bar{u}_x\}\\ \{\Delta \bar{u}_y\}\end{Bmatrix}$$

$$\{\Delta \bar{u}_x\}^T = \langle \Delta \bar{u}_{x1}, \Delta \bar{u}_{x2}, \ldots, \Delta \bar{u}_{x8}\rangle$$

$$\{\Delta \bar{u}_y\}^T = \langle \Delta \bar{u}_{y1}, \Delta \bar{u}_{y2}, \ldots, \Delta \bar{u}_{y8}\rangle$$

$$\langle h\rangle = \langle h_1, h_2, \ldots, h_8\rangle$$

$$h_1 = \frac{1}{4}(1+r)(1+s) - \frac{1}{4}(1-r^2)(1+s) - \frac{1}{4}(1+r)(1-s^2) \qquad h_5 = \frac{1}{2}(1-r^2)(1+s)$$

$$h_2 = \frac{1}{4}(1-r)(1+s) - \frac{1}{4}(1-r^2)(1+s) - \frac{1}{4}(1-r)(1-s^2) \qquad h_6 = \frac{1}{2}(1-r)(1+s^2)$$

$$h_3 = \frac{1}{4}(1-r)(1-s) - \frac{1}{4}(1-r)(1-s^2) - \frac{1}{4}(1-r^2)(1-s) \qquad h_7 = \frac{1}{2}(1-r^2)(1-s)$$

$$h_4 = \frac{1}{4}(1+r)(1-s) - \frac{1}{4}(1-r^2)(1-s) - \frac{1}{4}(1+r)(1-s^2) \qquad h_8 = \frac{1}{2}(1+r)(1-s^2)$$

Figure 2.1 Two-dimensional 8-node isoparametric element

3. FORMULATIONS OF STRUCTURAL EQUILIBRIUM EQUATIONS FOR BEAM ELEMENT

The Equation 2.9, derived for continuum element, can be applied to the beam elements. The influence of the geometric nonlinear stiffness matrix $[K^{nl}]$ in Equation 2.9 is negligible when the displacement increments are small. Thus the global static equilibrium equations for the beam in Updated Lagrangian formulation is given by

$$[K^l]\ \{\Delta \bar{U}\} = \{P\}_n - \{R\}_{n-1} \tag{3.1}$$

The structural stiffness matrix $[K^l]$ and internal resisting load vector $\{R\}_{n-1}$ in the global coordinate system can be obtained by rotating element stiffness matrix $[k^{*l}]$ and element internal resisting load vector $\{r^*\}_{n-1}$ in local coodinate system.

$$[K^l] = \sum [R]^T_{n-1}\ [k^{*l}]\ [R]_{n-1} \tag{3.2}$$

$$\{R\}_{n-1} = \sum [R]^T_{n-1}\ \{r^*\}_{n-1} \tag{3.3}$$

where

$$[k^{*l}] = \int_{V_{n-1}} [B^{*l}]^T_{n-1}\ [D^{*ep}]\ [B^{*l}]_{n-1}\ dV \tag{3.4}$$

$$\{r^*\}_{n-1} = \int_{V_{n-1}} [B^{*l}]^T_{n-1}\ \{\sigma^*\}_{n-1}\ dV \tag{3.5}$$

The elasto-plastic matrix $[D^{*ep}]$ in Equation 3.4 relates the local beam stress increment $\{\Delta\sigma^*\}$ to the local beam strain increment $\{\Delta\epsilon^{*l}\}$.

$$\{\Delta\sigma^*\} = [D^{*ep}]\ \{\Delta e^{*l}\} \tag{3.6}$$

Displacement increments $\{\Delta u^*\}$ and strain increments $\{\Delta e^{*l}\}$ can be expressed in terms of the element nodal displacement increments.

$$\{\Delta u^*\} = [N]_{n-1}\ \{\Delta \bar{u}^*\} \tag{3.7}$$

$$\{\Delta e^{*l}\} = [B^{*l}]_{n-1}\ \{\Delta \bar{u}^*\} \tag{3.8}$$

For 2-D plane beam element, element local and global degrees of freedom are shown in Figure 3.1 along with rotation matrix. Shape functions are given in Table 3.1. The shape functions in Table 3.1 assume cubic variation of flexure, quadratic variation of axial displacement and linear variation of shear rotations. It should be noted that the last three element nodal degrees of freedom $\langle \Delta\bar{u}_7, \Delta\gamma_8 \& \Delta\gamma_9 \rangle$ are independent of the adjoining elements and they are eliminated by static condensation prior to assembling the element matrices.

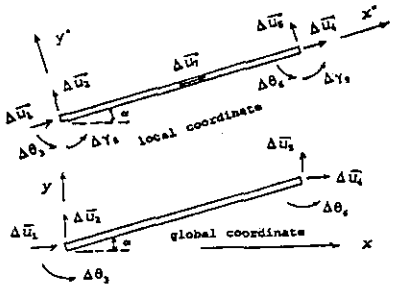

$$\{\Delta\bar{u}^*\} = [R]_{n-1}\{\Delta\bar{u}\}$$

$$[k^{*1}] = [R]_{n-1}^T [k^{*1}] [R]_{n-1}$$

$$[R]_{n-1} = \begin{bmatrix} [r] & [o] \\ [o] & [r] \end{bmatrix}$$

$$[r] = \begin{bmatrix} \cos\alpha & \sin\alpha & 0 \\ -\sin\alpha & \cos\alpha & 0 \\ 0 & 0 & 1 \end{bmatrix}$$

Figure 3.1 Degrees of freedom and rotation matrix for beam element.

$$\Delta u_x^* = h_1\Delta\bar{u}_1^* + h_7\Delta\bar{u}_7^* + h_4\Delta\bar{u}_4^* - y^*\left[h_{1,x^*}\Delta\bar{u}_2^* + h_{5,x^*}\Delta\bar{u}_5^* + h_{3,x^*}(\Delta\theta_3 + \Delta\gamma_8) + h_{6,x^*}(\Delta\theta_6 + \Delta\gamma_9) - (h_8\Delta\gamma_8 + h_9\Delta\gamma_9)\right]$$

$$\Delta u_y^* = h_2\Delta\bar{u}_2^* + h_5\Delta\bar{u}_5^* + h_3(\Delta\theta_3 + \Delta\gamma_8) + h_6(\Delta\theta_6 + \Delta\gamma_9)$$

$$\begin{Bmatrix} \Delta u_x^* \\ \Delta u_y^* \end{Bmatrix} = \begin{bmatrix} N_{x^*1}, N_{x^*2}, \ldots, N_{x^*9} \\ N_{y^*1}, N_{y^*2}, \ldots, N_{y^*9} \end{bmatrix}_{n-1}\{\Delta\bar{u}^*\}$$

$$h_1 = (2(\frac{x^*}{L})-1)\ ((\frac{x^*}{L})-1) \qquad h_5 = 3(\frac{x^*}{L})^2 - 2(\frac{x^*}{L})^3$$

$$h_2 = 1 - 3(\frac{x^*}{L})^2 + 2(\frac{x^*}{L})^3 \qquad h_6 = -L((\frac{x^*}{L})^2 - (\frac{x^*}{L})^3)$$

$$h_3 = L((\frac{x^*}{L}) - 2(\frac{x^*}{L})^2 + (\frac{x^*}{L})^3) \qquad h_7 = -4(\frac{x^*}{L})\ ((\frac{x^*}{L})-1)$$

$$h_4 = (\frac{x^*}{L})\ (2(\frac{x^*}{L})-1) \qquad h_8 = 1 - (\frac{x^*}{L})$$

$$h_9 = (\frac{x^*}{L})$$

Table 3.1 Shape functions for beam element.

In general, a beam element can be composed of composite sections with a set of reinforcing bars as shown in Figure 3.2. A beam section can be divided into top (flange) and bottom (web) subsections. Each subsection can be further divided into a number of layers. Numerical integration points are selected such that along the axis of beam, Gauss points are used and through the depth of the beam, the center points of each layer and each reinforcing bar are used as shown in Figure 3.2. The strain compatibilities along the boundary of subsections and between the plain body of beam and the reinforcing bar are assumed. Different material property sets can be specified to the top and bottom subsections of beam. Element stiffness matrix $[k^{*1}]$ and element internal resisting force vector $\{r^*\}_{n-1}$ can be computed using the equations listed in Table 3.2.

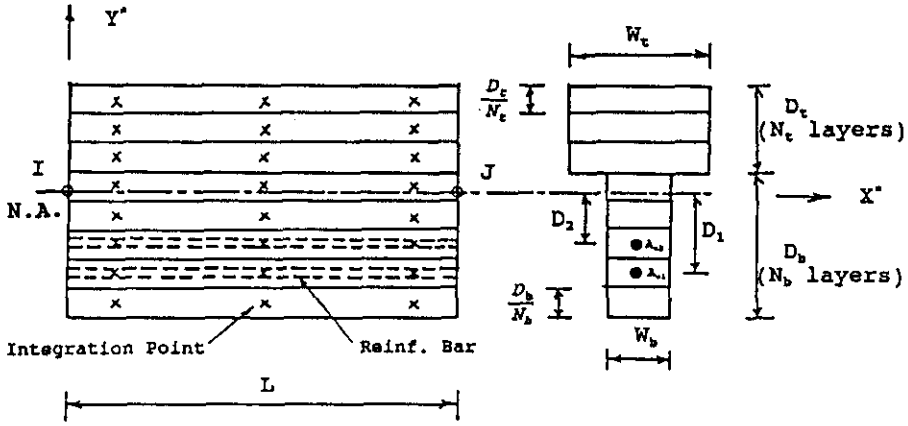

Figure 3.2 Schematic section view of layered reinforced beam.

$$[k^*] = \sum_{j=1}^{N_g} H_j \left\{ \sum_{i=1}^{N_b} \left(\frac{D_b}{N_b}\right) [B^{*-1}(x_j^*, y_i^*)]_{n-1}^T [D_b^{*ep}(x_j^*, y_i^*)] [B^{*-1}(x_j^*, y_i^*)]_{n-1} + \sum_{i=N_b+1}^{N_b+N_t} \left(\frac{D_t}{N_t}\right) [B^{*-1}(x_j^*, y_i^*)]_{n-1}^T [D_t^{*ep}(x_j^*, y_i^*)] [B^{*-1}(x_j^*, y_i^*)]_{n-1} + \sum_{i=1}^{N_r} A_{si} [B^{*-1}(x_j^*, y_i^*)]_{n-1}^T [D_r^{*ep}(x_j^*, y_i^*)] [B^{*-1}(x_j^*, y_i^*)]_{n-1} \right\}$$

$$\{r^*\}_{n-1} = \sum_{j=1}^{N_g} H_j \left\{ \sum_{i=1}^{N_b} \left(\frac{D_b}{N_b}\right) [B^{*-1}(x_j^*, y_i^*)]_{n-1}^T \{\sigma^*(x_j^*, y_i^*)\}_{n-1} + \sum_{i=N_b+1}^{N_b+N_t} \left(\frac{D_t}{N_t}\right) [B^{*-1}(x_j^*, y_i^*)]_{n-1}^T \{\sigma^*(x_j^*, y_i^*)\}_{n-1} + \sum_{i=1}^{N_r} A_{si} [B^{*-1}(x_j^*, y_i^*)]_{n-1}^T \{\sigma_r^*(x_j^*, y_i^*)\}_{n-1} \right\}$$

where
- H_j : Weight associated with j^{th} Gauss point
- D_t : Depth of top (flange) subsection
- D_b : Depth of bottom (web) subsection
- A_{si} : Cross section area of i^{th} reinforcing bar
- N_g : Number of Gauss points along the axis of beam
- N_b : Number of layers for bottom (web) subsection
- N_t : Number of layers for top (flange) subsection
- N_r : Number of reinforcing bar set
- x_j^* : x coordinate of j^{th} Gauss point
- Y_i^* : y coordinate of the centerline of i^{th} layer or i^{th} reinforcing bar

Table 3.2 Stiffness matrix & internal resisting load vector for beam element.

4. FORMULATIONS OF STRUCTURAL EQUILIBRIUM EQUATIONS FOR TRUSS ELEMENT

The same formulation (Equation 2.9) as derived for continuum element has been used for the truss element in SMAP-S2. It is rewritten here for clarity.

$$([K^l] + [K^{nl}])\ \{\Delta\bar{U}\} = \{P\}_n - \{R\}_{n-1} \tag{4.1}$$

Since the truss element contains only the axial stress along the axis of the member, the element stiffness matrices and the internal resisting force vector can be readily formulated in the element local coordinate system and then be transformed to the global coordinate system. Thus

$$[K^l] = \sum [R]^T_{n-1}\ [k^{*l}]\ [R]_{n-1} \tag{4.2}$$

$$[K^{nl}] = \sum [R]^T_{n-1}\ [k^{*nl}]\ [R]_{n-1} \tag{4.3}$$

$$\{R\}_{n-1} = \sum [R]^T_{n-1}\ \{r^*\}_{n-1} \tag{4.4}$$

where

$$[k^{*l}] = \int_{V_{n-1}} \langle B^{*l}\rangle^T_{n-1}\ E^{ep}\ \langle B^{*l}\rangle_{n-1}\ dV \tag{4.5}$$

$$[k^{*nl}] = \int_{V_{n-1}} [B^{*nl}]^T_{n-1}\ [\sigma_{x^*x^*}]_{n-1}\ [B^{*nl}]_{n-1}\ dV \tag{4.6}$$

$$\{r^*\}_{n-1} = \int_{V_{n-1}} \langle B^{*l}\rangle^T_{n-1}\ (\sigma_{x^*x^*})_{n-1}\ dV \tag{4.7}$$

The elasto-plastic Young's modulus E^{ep} in Equation 4.5 relates the axial stress increment $\Delta\sigma_{x^*x^*}$ to the axial strain increment $\Delta e^l_{x^*x^*}$.

$$\Delta\sigma_{x^*x^*} = E^{ep}\ \Delta e^l_{x^*x^*} \tag{4.8}$$

Displacement increment $\{\Delta u^*\}$ and strain increment $\Delta e^l_{x^*x^*}$ can be expressed in terms of the element nodal displacement increments.

$$\{\Delta u^*\} = [N]_{n-1}\ \{\Delta\bar{u}^*\} \tag{4.9}$$

$$\Delta e^l_{x^*x^*} = \langle B^{*l}\rangle_{n-1}\ \{\Delta\bar{u}^*\} \tag{4.10}$$

For 2-D plane truss element, element local and global degrees of freedom are shown in Figure 4.1 along with rotation matrix. Shape functions and element stiffness matrix in the local coordinate system are given in Table 4.1. It is assumed that the cross section area (A) remains constant during the deformation of truss member.

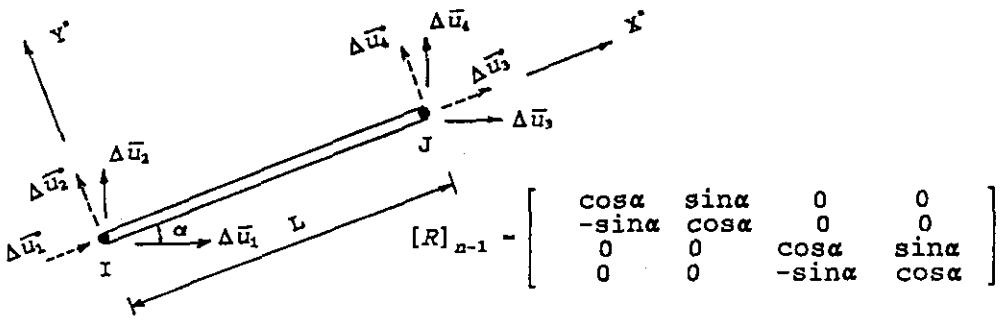

Figure 4.1 Degrees of freedom and rotation matrix for truss element.

$$\{\Delta u^*\} = [N]_{n-1} \{\Delta \bar{u}^*\}$$

$$\begin{Bmatrix} \Delta u_{x^*} \\ \Delta u_{y^*} \end{Bmatrix} = \begin{bmatrix} (1-\frac{x^*}{L}) & \frac{x^*}{L} & 0 & 0 \\ 0 & 0 & (1-\frac{x^*}{L}) & \frac{x^*}{L} \end{bmatrix} \begin{Bmatrix} \Delta \bar{u}_1^* \\ \Delta \bar{u}_2^* \\ \Delta \bar{u}_3^* \\ \Delta \bar{u}_4^* \end{Bmatrix}$$

$$[k^{*l}] = \frac{E^{ep} A}{(L)_{n-1}} \begin{bmatrix} 1 & 0 & -1 & 0 \\ 0 & 0 & 0 & 0 \\ -1 & 0 & 1 & 0 \\ 0 & 0 & 0 & 0 \end{bmatrix} \qquad [k^{*nl}] = \frac{\sigma_{x^*x^*} A}{(L)_{n-1}} \begin{bmatrix} 1 & 0 & -1 & 0 \\ 0 & 1 & 0 & -1 \\ -1 & 0 & 1 & 0 \\ 0 & -1 & 0 & 1 \end{bmatrix}$$

Table 4.1 Shape functions and stiffness matrix for truss element.

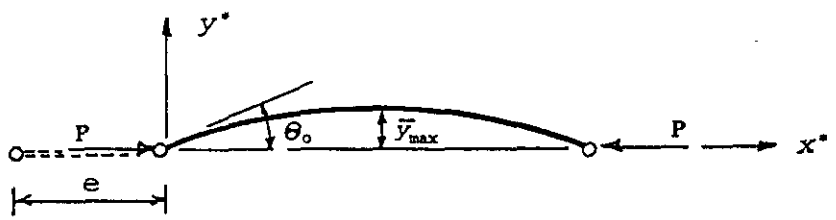

Figure 4.2 Laterally deflected truss member.

Post Buckling Behavior

Figure 4.2 shows the shape of the laterally deflected truss member. The axial force (P) - axial contraction (e) relationship can be derived by the finite deflection theory.

$$\frac{P}{(\frac{EI}{L^2})} = \alpha_0^2 \tag{4.11}$$

and

$$\frac{e}{L} = (1 - \frac{\beta}{\alpha_0}) \tag{4.12}$$

where

$$\alpha_0 = 2\int_0^{\frac{\pi}{2}} \frac{d\phi}{\sqrt{1 - k^2\sin^2\phi}} \qquad k = \sin\frac{\theta_0}{2}$$

$$\beta = 2\int_0^{\frac{\pi}{2}} \frac{(1 - 2k^2\sin^2\phi)\ d\phi}{\sqrt{1 - k^2\sin^2\phi}} \tag{4.13}$$

The nonlinear force-contraction curve can be developed by integrating Equation 4.13 for the given value of θ_0.
It should be noted that the force-contraction relationship in Equation 4.11 and 4.12 is valid until the maximum extreme fiber stress ($\bar{\sigma}_{max}$) at the midspan reaches the uniaxial yield stress (σ_{yield}) of the member. $\bar{\sigma}_{max}$ is given by

$$\bar{\sigma}_{max} = 2\ E\ L\ \bar{y}_{max}\ \alpha_0\ k \tag{4.14}$$

where $\bar{y}_{max}$ is the maximum distance from the neutral axis to the extreme fiber.

5. DESCRIPTION OF ELASTO-PLASTIC MATERIAL MODEL

SMAP employs the elasto-plastic material model developed by Kim, Piepenburg and Merkle (1986). The material model is based on theory of plasticity with the associated flow rule. The model in a generalized form can simulate Von Mises, Mohr-Coulomb, Drucker-Prager, and In situ rock (Generalized Hoek and Brown) models.

Failure Equation

The generalized form of failure equation is given by

$$F(p,\ q,\ \theta) = q - \{(\alpha + \beta p)^n + \kappa\}\ R(\theta) = 0 \tag{5.1}$$

where

$$p = \frac{1}{3}\sigma_{ii}$$

$$s_{ij} = \sigma_{ij} - p\delta_{ij}$$

$$J_2 = \frac{1}{2} s_{ij} s_{ij}$$

$$J_3 = \frac{1}{3} s_{ij} s_{jk} s_{ki}$$

$$q = \sqrt{3 J_2}$$

$$\theta = \frac{1}{3} \sin^{-1}\left(-\frac{27}{2} \frac{J_3}{q^3}\right)$$

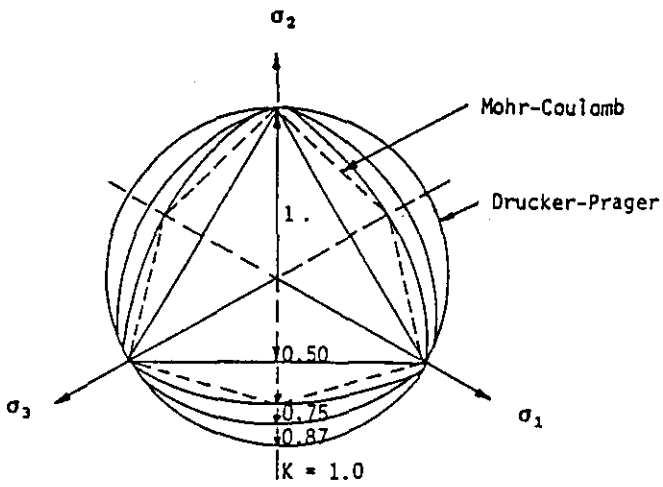

Figure 5.1 Shape of strength envelope, $R(\theta)$, on octahedral plane.

Elastic Stress-Strain Relationship

The incremental elastic constitutive law can be expressed in the following matrix form:

$$\{d\sigma\} = [D^e]\ \{de^e\} \qquad (5.2)$$

where $\{de^e\}$ is the elastic strain increment.

Yield Surface

The material model does not allow hardening. Thus the yield surface coincides with the failure surface as given by Equation 5.1. Materials behave elastically under the failure surface, and perfectly plastic on the failure surface. The expression for $R(\theta)$ in Equation 5.1 is given by

$$R(\theta) = \frac{x(\sqrt{3}\cos\theta+\sin\theta)+(2k-1)\left[(2+\cos2\theta+\sqrt{3}\sin2\theta)x + 5k^2-4k\right]^{\frac{1}{2}}}{\left[x(2+\cos2\theta + \sqrt{3}\sin2\theta) + (1-2k)^2\right]} \qquad (5.3)$$

$$(-\frac{\pi}{6} \leq \theta \leq \frac{\pi}{6})$$

where $x = (1 - k^2)$ and k is the ratio of the shear strength in triaxial extension to the shear strength in triaxial compression at the same mean pressure. As shown in Figure 5.1, $R(\theta)$ varies from a smooth-cornered triangle to a circle depending on the value of k.

Flow Rule

An associated flow rule is assumed. Thus the plastic strain increment, $\{d\varepsilon^p\}$, is in the direction normal to the failure surface, which will allow dilatancy at failure. In mathematical terms

$$\{d\varepsilon^p\} = d\lambda\{a\} \tag{5.4}$$

where $d\lambda$ is the non-negative proportionality constant and $\{a\}$ is the column vector of derivatives of the yield function with respect to the stress components.

$$\{a\} = \{\frac{\partial F}{\partial \sigma}\}$$

Consistency Equation

During Yielding, the consistency equation forces the stress to move along the yield surface.

$$dF = \{a\}^T \{d\sigma\} = 0 \tag{5.5}$$

Incremental Elasto-plastic Constitutive Law

Total strain is defined as the sum of elastic and plastic strains

$$\{d\varepsilon\} = \{d\varepsilon^e\} + \{d\varepsilon^p\} \tag{5.6}$$

Substituting Equation 5.6 into 5.2, we have

$$\{d\sigma\} = [D^e](\{d\varepsilon\} - \{d\varepsilon^p\}) \tag{5.7}$$

From the flow rule defined in Equation 5.4, we can rewrite Equation 5.7 as

$$\{d\sigma\} = [D^e]\{d\varepsilon\} - d\lambda\,[D^e]\,\{a\} \tag{5.8}$$

Now substituting Equation 5.8 into Equation 5.5 and solving for $d\lambda$, we obtain

$$d\lambda = \frac{\{a\}^T [D^e]\,\{d\varepsilon\}}{\{a\}^T [D^e]\,\{a\}} \tag{5.9}$$

Backsubstituting this $d\lambda$ into Equation 5.8, the stress increment is directly related to the total strain increment as follows:

$$\{d\sigma\} = [D^{ep}]\,\{d\varepsilon\} \tag{5.10}$$

Where the incremental elasto-plastic constitutive matrix is expressed as

$$[D^{ep}] = [D^e] - \frac{[D^e]\,\{a\}\,\{a\}^T [D^e]}{\{a\}^T [D^e]\,\{a\}} \tag{5.11}$$

Determination of Material Parameters

The constant, n, determines the type of strength envelope in the p-q plane. Table 5.1 shows the material parameters and required tests. For $n=\frac{1}{2}$, the model represents the generalized Hoek and Brown model which is based on extensive field and laboratory data. The material parameters for this empirical model are tabulated in Table 5.2 for several different rock types as a function of rock quality.

Table 5.1 Material parameters and required tests.

n	Required tests	Strength envelope in terms of major and minor principal stresses	Material constants for model (α, β, κ, and K)	Remarks
0	Uniaxial stress	$\sigma_1 - \sigma_3 = \bar{q}$ $\bar{q}$: uniaxial yield stress	α and β are arbitrary $\kappa = \bar{q} - 1$ $K = 1$	VON MISES MODEL
½	Triaxial compression Triaxial extension	$\sigma_1 - \sigma_3 = (m\,\sigma_c\sigma_3 + s\,\sigma_c^2)^{1/2}$ σ_c : unconfined compression strength of intact rock m and s are material constants depending on rock type and quality (ex. discontinuity spacing)	$\alpha = (\frac{m^2}{32} + s)\,\sigma_c^2$ $\beta = \frac{m}{8}\,\sigma_c$ $\kappa = \frac{1}{4}\,m\,\sigma_c$ $K = \frac{q_e}{q_c}$ q_e and q_c are triaxial extension and compression shear strengths respectively, measured at the same mean pressure	GENERALIZED HOEK AND BROWN MODEL Approximate values of m and s are available from the empirical data base by Hoek and Brown
1	Triaxial compression Triaxial extension	$\sigma_1 - \sigma_3 = (\sigma_1 + \sigma_3)\sin\phi + 2c\cos\phi$ ϕ : internal friction angle c : cohesion	$\alpha + \kappa = \frac{6\cos\phi}{3-\sin\phi}\,c$ $\beta = \frac{6\sin\phi}{3-\sin\phi}$ $K = \frac{q_e}{q_c}$	MODIFIED MOHR-COULOMB MODEL For Drucker-Prager Model $K = 1$ For Smooth-cornered Mohr-Coulomb Model $K = \frac{3-\sin\phi}{3+\sin\phi}$

Table 5.2 Hoek and Brown material parameters.

Rock Type / Rock Quality	Dolomite, Limestone and Marble	Mudstone, Siltstone, Shale and Slate (Normal to Cleavage)	Sandstone and Quartzite	Andesite, Dolerite, Diabase and Rhyolite	Amphibolite, Gabbro, Gneiss, Granite, Norite and Quartz-Diorite
INTACT CSIR rating = 100 NGI rating = 500	m = 7. s = 1.	10. 1.	15. 1.	17. 1.	25. 1.
VERY GOOD QUALITY CSIR rating = 85 NGI rating = 100	3.5 0.1	5. 0.1	7.5 0.1	8.5 0.1	12.5 0.1
GOOD QUALITY CSIR rating = 65 NGI rating = 10	0.7 0.004	1.0 0.004	1.5 0.004	1.7 0.004	2.5 0.004
FAIR QUALITY CSIR rating = 44 NGI rating = 1	0.14 0.0001	0.20 0.0001	0.3 0.0001	0.34 0.0001	0.5 0.0001
POOR QUALITY CSIR rating = 23 NGI rating = 0.1	0.04 0.00001	0.05 0.00001	0.08 0.00001	0.09 0.00001	0.13 0.00001
VERY POOR QUALITY CSIR rating = 3 NGI rating = 0.01	0.007 0.	0.01 0.	0.015 0.	0.017 0.	0.025 0.

Description of Rock Quality

INTACT ROCK SAMPLES : Laboratory size specimens free from joints.

VERY GOOD QUALITY ROCK MASS : Tightly interlocking undisturbed rock with unweathered joints at 1 to 3m.

GOOD QUALITY ROCK MASS : Fresh to slightly weathered rock, slightly disturbed with joints at 1 to 3m.

FAIR QUALITY ROCK MASS : Several sets of moderately weathered joints spaced at 0.3 to 1m.

POOR QUALITY FOCK MASS : Numerous weathered joints at 30 to 500mm with sane gouge. Clean compacted waste rock.

VERY POOR QUALITY ROCK MASS : Numerous heavily weathered joints spaced < 50mm with gouge. Waste rock with fines.

6. MULTI-STAGED EXCAVATION AND CONSTRUCTION SIMULATION

The sequence of excavation or construction events has a significant influence on the final states of stress and displacement fields. The source of nonlinearity in this case comes from the geometry or boundary change. Therefor the general nonlinear solution scheme can be used.

SMAP has an option of element activity to simulate the excavation or construction sequence. For those elements to be excavated, they are active initially and are deactive at a designated step when excavation occurs. For those elements to be

constructed, such as support systems, they are deactive initially and are active at a designated step when the installation takes place. For those elements to be constructed temporarily, such as temporary support system, they are active at a step when installed and are deactive at a step when removed.

7. CODE VERIFICATION

Code verfication is essencial to check the validity of implementations. A complete set of verification problems were presented in SMAP-S2 User's Manual. In this paper, only four verification problems are selected to show the validity of the implemented algorithms associated with the geometric and material nonlinearities.

The first problem is to analyze a ten-foot diameter unlined circular tunnel subjected to a uniform free field stress of 2800 psi. This problem is to verify both the Drucker-Prager model and the axisymmetric elements in SMAP-S2. The semi-analytical solution, FDAXP, for this problem was derived by Kim & Davister (1986). Computed tangential stress profile is shown in Figure 7.1. As seen, SMAP results agree well with the semi-analytical solution.

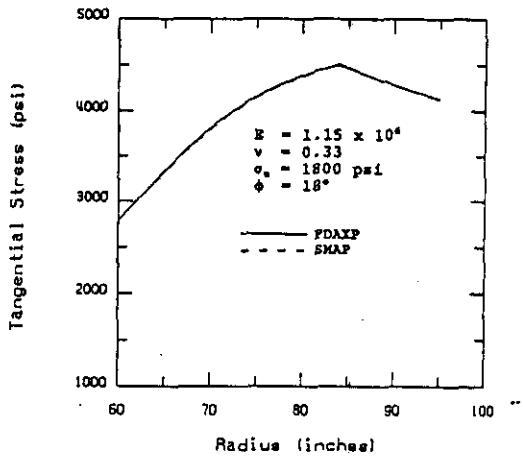

Figure 7.1 Axisymmetric tunnel.

The second problem is to solve classic problem of a rigidly jointed toggle as shown in Figure 7.2. This problem is to verify geometric nonlinearity in SMAP as formulated for beam elements. For this toggle, the closed form solution as well as experimental results was obtained by Williams (1964). By symmetry, only the left half of the structure is modeled using 10 beam elements. The load-deflection response at midspan is shown in Figure 7.2. SMAP results agree very well with the closed form solution.

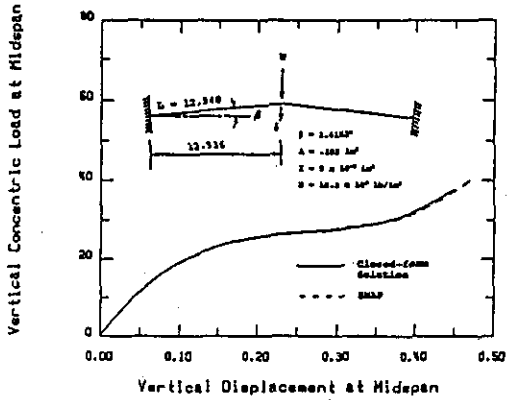

Figure 7.2 William's toggle.

The third problem is to compute the response of Burns and Siess' beam shown in Figure 7.3. This problem is to verify concrete cracking, steel bar yielding, and concrete crushing as concentrated load at midspan is increased monotonically to failure. By symmetry only right half of the structure is modeled using 22 beam elemnents. Load-deflection response at midspan is shown in Figure 7.3. As seen, there is very good agreement between the experimental and SMAP results.

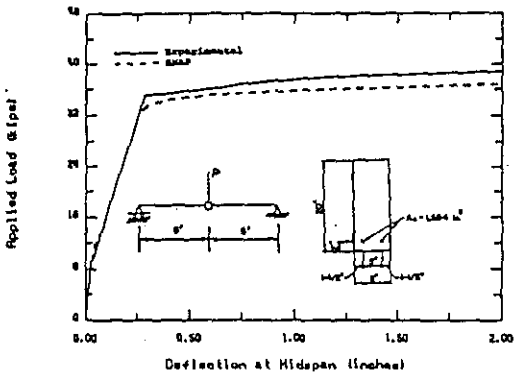

Figure 7.3 Burns and Siess' beam.

The last verification problem is to calculate the response of buckled truss. As shown in Figure 7.4, a vertical load, W, is applied monotonically until the structure buckles significantly. In fact, only the bottom member shortens and buckles while the top member elongates continuously. This problem is to check the post-buckling behavior of truss member. Both theoretical closed form solution and experimental test result are presented by Britvec (1973). As seen in Figure 7.4, SMAP results are nearly identical to the closed form solution, but they are slightly higher than experimental test results.

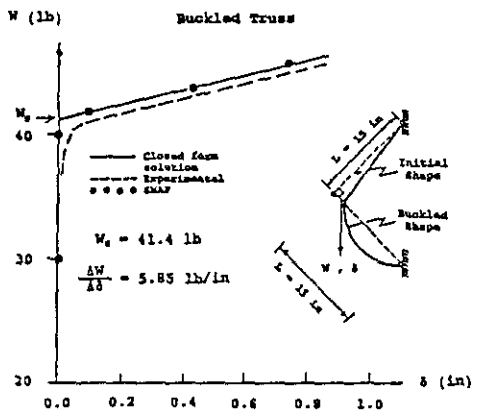

Figure 7.4 Buckled truss.

8. PRE- AND POST-PROCESSING FEATURES

Shown in Figure 8.1 is the pre- and post-processing program structure of SMAP-S2. In the following, the features of pre- and post-processing programs will be described briefly:

GBLOCK:

Program GBLOCK generates block nodal coordinate for two consecutive blocks. The first block represents near field zone where the soil or rock medium undergoes the major disturbance. And the second block represents far field zone. Note that GBLOCK

stores the block nodal coordinates which can be an input for PRESMAP1 or PRESMAP2.

PRESMAP 1 & 2:

PRESMAP1 and PRESMAP2 are the pre-processor for SMAP-S2. These pre-processing programs are used to automatically generate nodal coodinates, indexes, and nodal loads for continuum element.

PLTDS:

PLTDS is the post-processor for SMAP-S2.
Graphical outputs produced by PLTDS include

- Finite element mesh,
- Deformed shape,
- Principal stress distribution,
- Section forces in beam element,
- Extreme fiber stresses/strains in beam elements, and
- Axial force/stress/strain in truss elements

Graphical outputs will be either displayed on the screen or directly sent to the hardcopy device such as dot matrix printer, laser printer, and plotter.

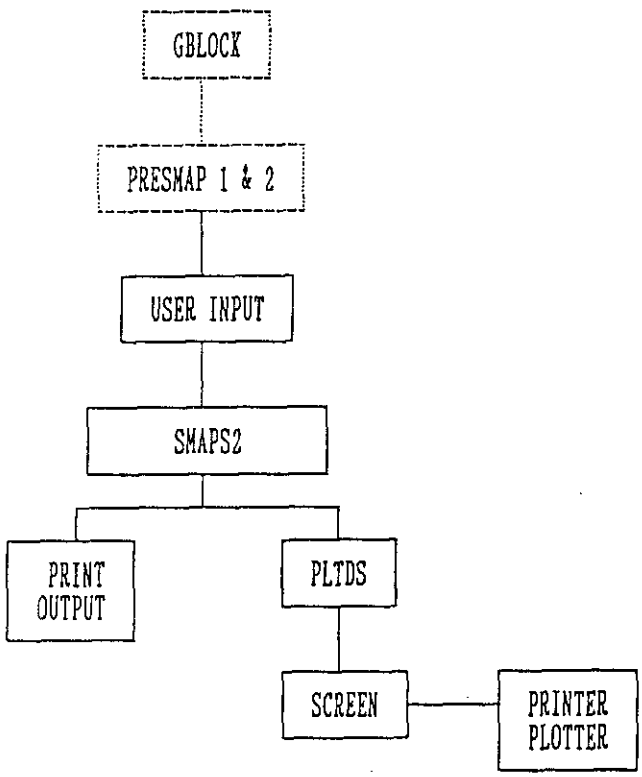

Figure 8.1 Pre-and post-processing structure of SMAP-S2

9. CONCLUDING REMARKS

SMAP-S2 is an advanced two-dimensional, static, nonlinear structure-medium analysis program. Practical applications of the program include underground structural analysis for tunnels, shafts, caverns, chambers, etc. Theoretical equations and some capabilities of the program are presented. Verifications are performed to check the geometric and material nonlinear features of the program.

Special features of SMAP-S2 are as follows:

- Large deformations and material inelasticity are considered.
- Multi-staged excavation or construction simulation is allowed.
- Empirical-based Hoek and Brown model is employed to model in situ rock mass.
- Reinforced concrete and composite structures are explicitly modeled by beam element.
- Post bucklings as well as yieldings are allowed for truss element.
- Special mesh generating routines for tunnel analysis are provided.
- Graphical output for stresses, strains, and deformations are automatically scaled and displayed on the screen, or plotted on the plotter, or printed on the dot-matrix and laser printers.

REFERENCE

1. Britvec, S.J. "The Stability of Elastic Systems", University of Stuttgart, Pergamon Press Inc, 1973.
2. Burns, N.H. and Siess, C.P., "Load-Deformation Characteristics of Beam-Column Connections in Reinforced Concrete, "Civil Engineering Studies, SRS No. 234, Univerisity of Illinois, Urbana, Il, January 1962.
3. COMTEC Research, "SMAP-S2 (Structure-Medium Analysis Program) User's Manual", Version 1, May 1991.
4. Hoek, E. and E.T. Brown, "Empirical Strength Criterion for Rock Masses", Journal of the Geotechnical Engineering Division, ASCE, vol. 106, No. GT9, September 1980.
5. Kim, K.J. and M. Davister, "Numerical Analysis of Nonlinear Liner-Medium Interaction", Volume II - Cylindrical Tunnel Subjected to Axisymmetric Loading, Prepared for Defence Nuclear Agency, Contract No. DNA 001-84-c-0149, July, 1987.
6. Kim, K.J., D.D. Piepenburg, and D. Merkle, "Influence of the Intermediate Principal Stress on Rock Tunnel Behavior", Applied Research Associates, Inc., Alexandria, VA, January 1986.
7. Williams, F.W., "An Approach to the Nonlinear Behavior of the Members of a Rigidly Jointed Plane Framework with Finite Deflections", Quarterly Journal of Mechanics and Applied Mathematics, Vol. 17, London, UK, 1964, pp. 451-469.